J. Earth Syst. Sci. (2020)129 93
https://doi.org/10.1007/s12040-020-1361-9

Iron limitation study in the North Indian Ocean using model simulations

M K Sharada*, C Kalyani Devasena and P S Swathi

CSIR-Fourth Paradigm Institute, NAL Belur Campus, Bengaluru 560 037, India.
**Corresponding author. e-mail: sharada@csir4pi.in*

MS received 1 July 2019; revised 20 December 2019; accepted 26 December 2019

There have been many studies on iron as a limiting nutrient for productivity in the World Ocean, but only a few studies have been done in the Arabian Sea on iron limitation. Sensitivity of primary productivity, chlorophyll, nitrate, pCO_2 and carbon flux in the Arabian Sea to one of the parameters related to iron limitation has been investigated using a three-dimensional coupled biogeochemical model (TOPAZ) embedded in Modular Ocean Model (MOM) in the global domain, for climatology and interannual variability. Initially, the model results are evaluated for many of the biogeochemical components using data from World Ocean Atlas, satellites and cruises in the Arabian Sea. It is noticed that model results capture spatial and temporal variations of some of the biogeochemical components and fluxes in the north Indian Ocean. Subsequently, it is shown that micronutrient iron plays a significant role on the growth of phytoplankton, utilization of nutrients, pCO_2 in the ocean and carbon flux across the air–sea interface in north and north-west regions of the Arabian Sea.

Keywords. Iron limitation; biogeochemical model; Arabian Sea; primary productivity; carbon flux; modelling and simulation.

1. Introduction

It is generally accepted that global warming is due to the increase in the emission of greenhouse gases including CO_2 to the atmosphere and reduction of these emissions are required in future (IPCC 2007). Carbon is transferred between the surface and deep ocean due to solubility of CO_2 in seawater and ocean circulation (solubility pump), and due to biological processes like primary production, settling of detritus, dispersion due to physical processes, etc. (biological pump). The effects of these two pumps on the carbon cycle are of comparable significance (Sarmiento *et al.* 1995). It is observed that effect of solubility pump is more now compared to pre-industrial times because emission of CO_2 to atmosphere is increased (IPCC 2007).

Cruise measurements of Joint Global Ocean Flux Studies (JGOFS) and other ocean observational programmes are inadequate for making basin-wide estimates of primary productivity and carbon flux. Therefore, it is essential to have robust well-tested three-dimensional (3D) mathematical models that incorporate biological and chemical processes in addition to physical processes for estimation of oceanic primary production, transport and sinking of organic matter from the euphotic zone. Such mathematical models help in understanding spatial and temporal variations of biogeochemical components and fluxes, and the interaction between the marine food web and biogeochemical cycles on global and regional scales. They also enable us to look at the dynamics of marine biogeochemical cycles at several time

Published online: 11 March 2020

scales: from diurnal variation to annual scales. These models will also allow us to ask 'What if?' questions. What if we fertilized the ocean by supplying limiting nutrients? Will this result in deep sequestration or will the organic matter be advected, remineralised and returned to the surface ocean elsewhere? What are the short term gains and long term ones?

It is well known that marine primary production is limited by availability of light and macro and micro nutrients. If there is an enhancement in the supply of the limiting nutrient, primary production is increased till some other nutrient limits the production. This feature of nutrient limitation for primary production leads to the suggestion that ocean fertilization could be used for changing the uptake of CO_2 due to biological pump.

Ocean fertilization can be used as a tool for increased uptake of carbon from atmosphere if carbon removed due to fertilization is not brought back to the ocean surface for more than a century (IPCC 2007). It was reported for the first time by Martin and Fitzwater (1988) and Martin *et al.* (1989), that enhancement in the supply of iron (Fe) to water at Ocean Station Papa (OSP) increased the growth of phytoplankton and consumption of nitrate. The findings of 12 Mesoscale Fe addition experiments (FeAXs) in high-nutrient, low-chlorophyll (HNLC) regions (the eastern equatorial Pacific, the ice-free Southern Ocean and the open subarctic north Pacific) have shown that primary production is limited by Fe in one-third of the world ocean, and Fe enrichment influences the biogeochemical cycles of various nutrients (carbon, nitrogen, silicon, sulphur, etc.), and hence the Earth Climate system (Boyd *et al.* 2007). Smetacek and Naqvi (2008) provided a detailed analysis related to the biomass created due to enhanced production, efficiency of Fe fertilization in removal of carbon and side effects of fertilization. It is pointed out by Smetacek and Naqvi (2008) and Buesseler *et al.* (2008) that most of the Fe fertilization experiments were not specifically designed to analyse the processes related to organic carbon uptake. The essential role of grazing control acting in concert with Fe limitation was emphasized by Cullen (1995).

Studies of regional circulation models embedded with biogeochemistry which are validated by the observations are required to understand the impact of Fe enrichment on climate. Many of the current marine ecosystem models have included iron limitation since Fe plays a key role in growth of phytoplankton, carbon and nitrogen cycles and community structure in the oceans, particularly in the HNLC regions.

Gnanadesikan *et al.* (2003) have studied the effects of patchy fertilization on atmospheric CO_2 and biological production using an ocean general circulation model. They have discussed in detail about micro and macro nutrient fertilization scenarios, effect of remineralization profiles on productivity and carbon flux, effect of fertilization over different time, and space scales, nonlocal effects of fertilization, to estimate the true environmental impact.

Though there have been many studies in the HNLC regions of the World Ocean, there are only a few studies on Fe limitation in the Arabian Sea (AS). Behrenfeld *et al.* (2009) have shown that there is Fe limitation in some regions of the AS in surface waters using remote sensing data. Distribution of trace elements like Fe, Al, etc., during three seasons in the AS using U.S. Joint Global Ocean Flux Studies (US JGOFS) cruise data have been studied by Measures and Vink (1999). Some of the biogeochemical models show Fe limitation (Wiggert and Murtugudde 2007) and some do not (Moore *et al.* 2004; Dutkiewicz *et al.* 2005; Resplandy *et al.* 2011). Therefore, a few more observations in the water column are required to get a better understanding of Fe limitation in the AS. It is observed that Fe concentration is very low and limits primary productivity (PP) in some regions of western AS during some seasons (SWM) and hence, Fe influences the biogeochemistry of AS, and this may be related to atmospheric dust deposition (Naqvi *et al.* 2010). A study was done on Fe distribution and the biological response to Fe addition in the AS and the results show that PP is limited by Fe during southwest monsoon in central AS (Moffett *et al.* 2015). There are a few studies on the enhancement of chlorophyll due to dust storms in the Arabian Sea (Kayetha *et al.* 2007; Singh *et al.* 2008; Gautam *et al.* 2009).

A description of the physical and biogeochemical model is provided in section 2.1 and the details of numerical simulations for parameter sensitivity of the coupled physical-biogeochemical model are given in section 2.2. Also, a summary of earlier studies on model evaluation is provided in section 2.2. In section 3, initially, discussion on the analysis of the model simulation results, model validation using data from satellites, cruises and World Ocean Atlas is given. Thereafter, using results of model simulations, biogeochemical

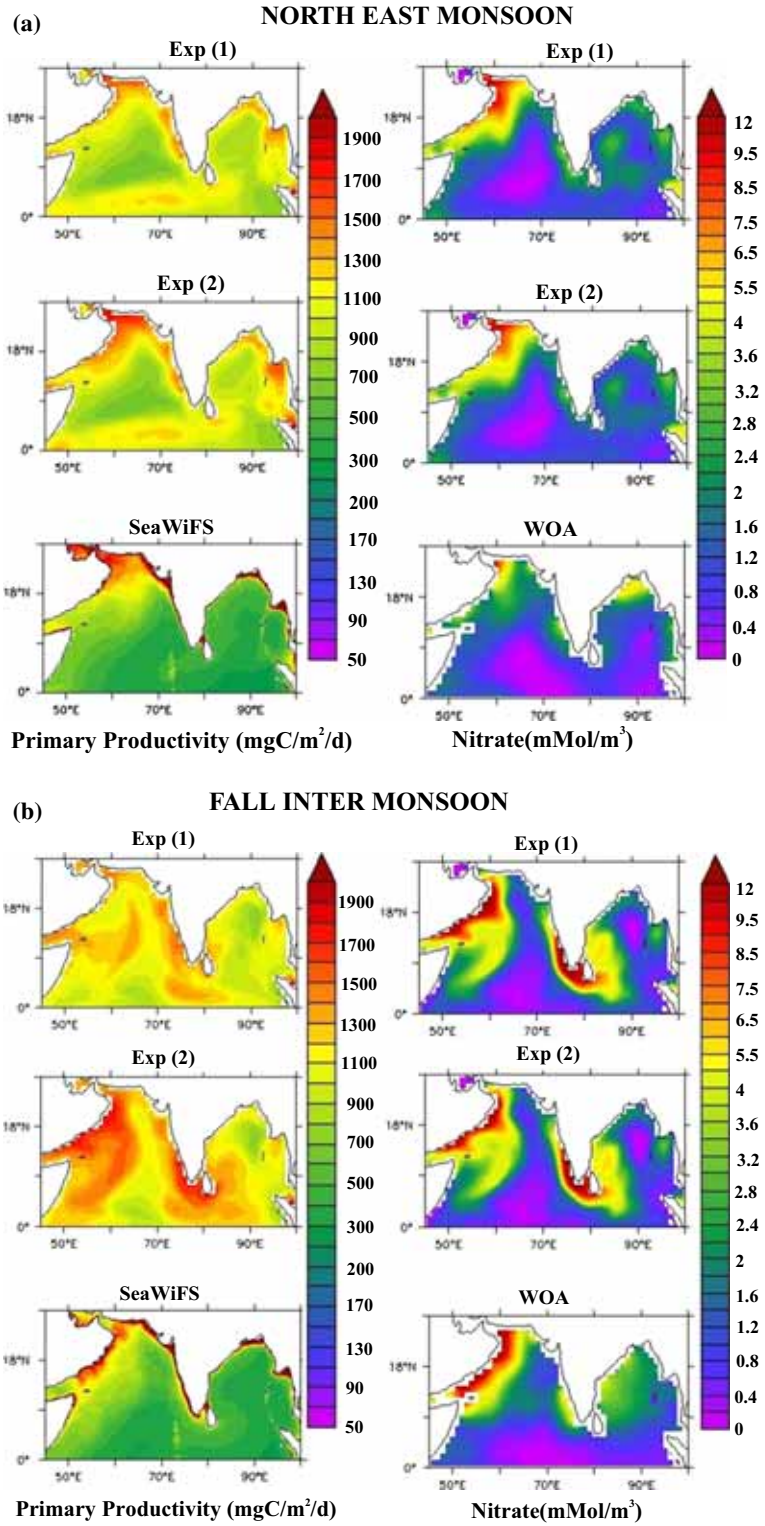

Figure 1. Spatial variation of primary productivity (PP) (mgC/m^2/d) in the euphotic zone and nitrate (mMol/m^3) in the upper 50 m during (**a**) Northeast Monsoon and (**b**) Fall Inter Monsoon for model simulations Exp (1) and (2) compared with PP estimated from SeaWiFS satellite data and Nitrate from WOA (2005) in the north Indian Ocean. (**c**) Spatial variation of pCO_2 (µatm) during two seasons in the north Indian Ocean for two numerical simulations Exp (1) – (i), (ii) and Exp (2) – (iii), (iv) compared with Takahashi pCO_2 atlas (2009) – (v), (vi).

variables and fluxes which are influenced by iron limitation are identified. Results of model simulations with interannual variability are analysed to understand the variations due to ENSO events. Based on model simulation results, effect of iron limitation on processes related to primary

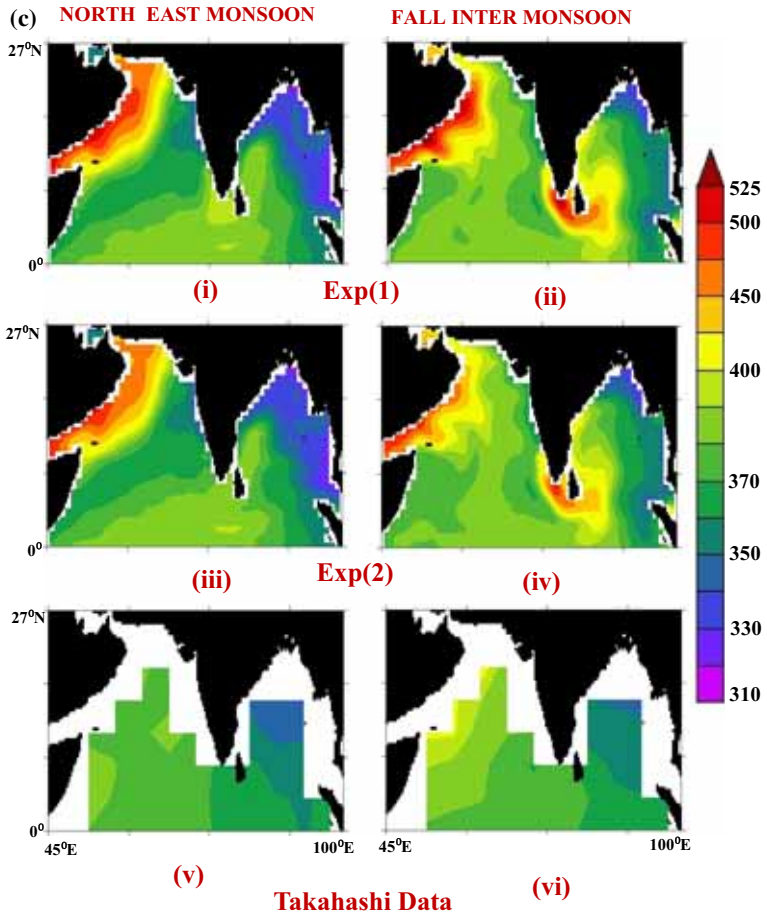

Figure 1. (*Continued.*)

productivity in different regions of Arabian Sea are analysed in detail.

2. Model and methodology

2.1 *Mathematical model*

The present study on the effects of nutrients on marine biogeochemical cycles including a micronutrient like iron is based on the numerical simulations of three-dimensional coupled biogeochemical model (Dunne *et al.* 2010, TOPAZ – Tracers of Phytoplankton with Allometric Zooplankton). The physical model is based on the Modular Ocean Model (MOM4P1: Griffies 2007) developed at the NOAA GFDL. The model set-up consists of 50 vertical levels, with 25 in the top 250 m to resolve the mixed layer properties. A detailed description of the model configuration used in this study can be found in Sharada *et al.* (2015) and only a short summary is provided here in the interest of continuity. The horizontal resolution of the model is 1° globally with 1/3° resolution near the equator. The physics of the model include k-pp parametrization for vertical diffusion of momentum and tracers (Large *et al.* 1994), and solar absorption by dynamically-computed chlorophyll. The numerics ensure that the positive-definiteness of the tracer transport operator is preserved in the advection scheme. The biogeochemical model TOPAZ developed at GFDL has been coupled with MOM4P1. This prognostic ocean biogeochemistry model contains a large number of tracers including three phytoplankton groups (diatoms, eukaryotic phytoplankton, diazotrophs), two forms of dissolved organic matter (labile and semi-labile), heterotrophic biomass, detritus, nutrients (Nitrogen – N, Phosphate – P, Silicate – Si and Iron – Fe), dissolved inorganic carbon and alkalinity. The model includes the ecological cycling of dissolved inorganic species for coupled Carbon (C), N, P, Si, Fe, Calcium Carbonate ($CaCO_3$), oxygen (O_2) and lithogenic cycling with flexible N:P:Fe stoichiometry. The growth rate of phytoplankton is calculated based on Geider *et al.* (1997). The interaction of biologically active elements and ecological cycling is modelled by the formulation of significant biogeochemical processes,

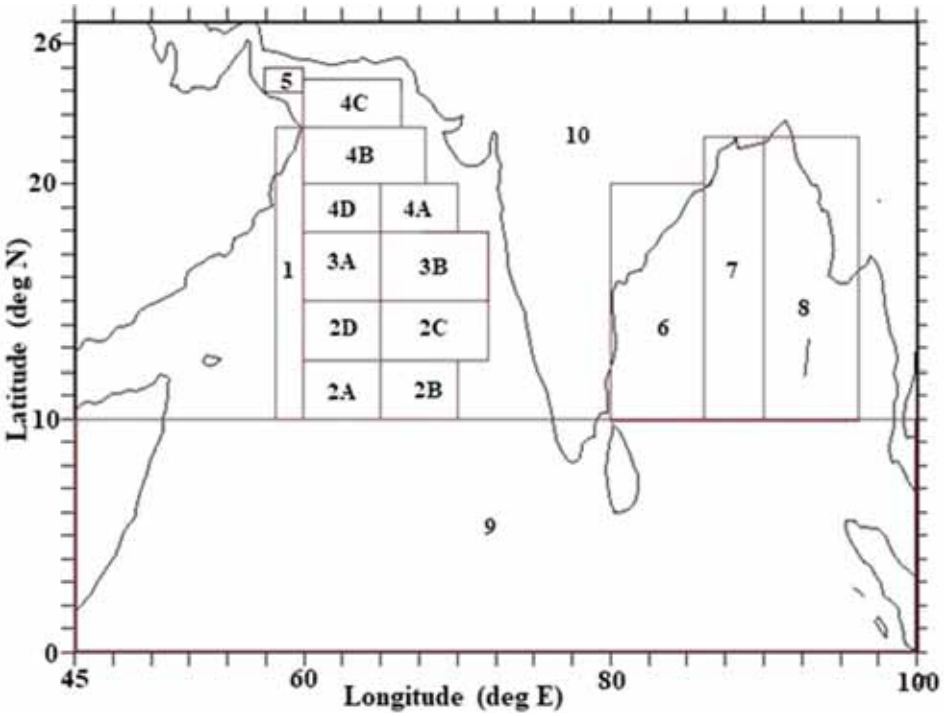

Figure 2. Biogeochemical provinces/regions in the Arabian Sea and the Bay of Bengal.

like multi-nutrient limitations including iron and silicate (Liebig), light limitation, ammonium inhibition (Sharada *et al.* 2005), food-web processing, grazing, remineralization, gas exchange, atmospheric deposition of iron, scavenging, N_2 fixation, denitrification, river inputs of lithogenic material, sediment processes, etc. The rate of change of tracers with respect to time at a given point in the global domain is determined using the tracer conservation equation which includes advection, diffusion and source and sink terms representing the biogeochemical processes.

Table 1. *Spatial extent of different biogeochemical provinces/regions in the Arabian Sea and Bay of Bengal.*

Region	Longitude	Latitude
1	58°–60°E	10°–22.5°N
2A	60°–65°E	10°–12.5°N
2B	65°–70°E	10°–12.5°N
2C	65°–72°E	12.5°–15°N
2D	60°–65°E	12.5°–15°N
3A	60°–65°E	15°–18°N
3B	65°–72.5°E	15°–18°N
4A	65°–70°E	18°–20°N
4B	60°–68°E	20°–22.5°N
4C	60°–66°E	22.5°–24.5°N
4D	60°–65°E	18°–20°N
5	57.5°–60°E	24°–25°N
6	80°–86°E	10°–20°N
7	86°–90°E	10°–22°N
8	90°–96°E	10°–22°N
9	45°–100°E	0°–10°N
10	45°–100°E	0°–27°N

2.2 *Numerical simulations*

Numerical simulations of the marine biogeochemical model (TOPAZ) is carried out for 200 yrs with climatological forcing and then forced with CORE v2 dataset (CLIVAR Working Group for Ocean Model Development-Dataset used for the Common Ocean-sea ice Reference Experiments: Griffies *et al.* 2009) in the global domain to study the sensitivity of one of the parameters related to iron limitation $(Fe:N)_{irr}$, on the marine biogeochemical cycle. For the present study, marine biogeochemical model simulations are carried out in the global domain for three different values of a parameter $(Fe:N)_{irr}$ (equations related to $(Fe:N)_{irr}$ are given in the appendix), which alters the light utilization efficiency for phytoplankton through chlorosis factor, namely, Exp (1), Exp (2) and Exp (3) during 1949–2009. These numerical simulation results are analysed in detail to investigate the sensitivity of the parameter $(Fe:N)_{irr}$ on Primary Productivity (PP), Chlorophyll (Chl), Nitrate (NO_3), pCO_2 and carbon flux in the AS. If $(Fe:N)_{irr}$ is high, there is Fe limitation, and when $(Fe:N)_{irr}$ is

decreased Fe limitation is reduced. Values of $[(\mathrm{Fe{:}N})_{\mathrm{irr}}]$ for large and small phytoplankton and diazotrophs for three numerical experiments are given below:

Exp (1): Control experiment

$$\left[(\mathrm{Fe{:}N})_{\mathrm{irr}}\right]_{\mathrm{di}} = 60 \times 10^{-6} \times 106/16\,\mathrm{mol\,Fe/mol\,N},$$
$$\left[(\mathrm{Fe{:}N})_{\mathrm{irr}}\right]_{\mathrm{sm}} = 10 \times 10^{-6} \times 106/16\,\mathrm{mol\,Fe/mol\,N},$$
$$\left[(\mathrm{Fe{:}N})_{\mathrm{irr}}\right]_{\mathrm{lg}} = 30 \times 10^{-6} \times 106/16\,\mathrm{mol\,Fe/mol\,N}.$$

Exp (2): $(\mathrm{Fe{:}N})_{\mathrm{irr}}$ reduced to one-fourth of the values compared to control experiment for small and large phytoplankton and diazotrophs.

Exp (3): $(\mathrm{Fe{:}N})_{\mathrm{irr}}$ reduced to half of the values compared to control experiment for small and large phytoplankton and diazotrophs.

In Exp (2) and Exp (3), iron limitation is reduced (see appendix) compared to control experiment. Results of numerical simulations of control experiment, Exp (1), have been analysed in detail in earlier studies by authors (Kalyani Devasena *et al.* 2014; Sharada *et al.* 2015). Results of climatological simulations of control experiment were validated for spatial and seasonal variations of sea surface temperature (SST), sea surface salinity (SSS), chlorophyll (Chl), primary productivity (PP), nitrate (NO_3), silicate, oxygen, pCO_2

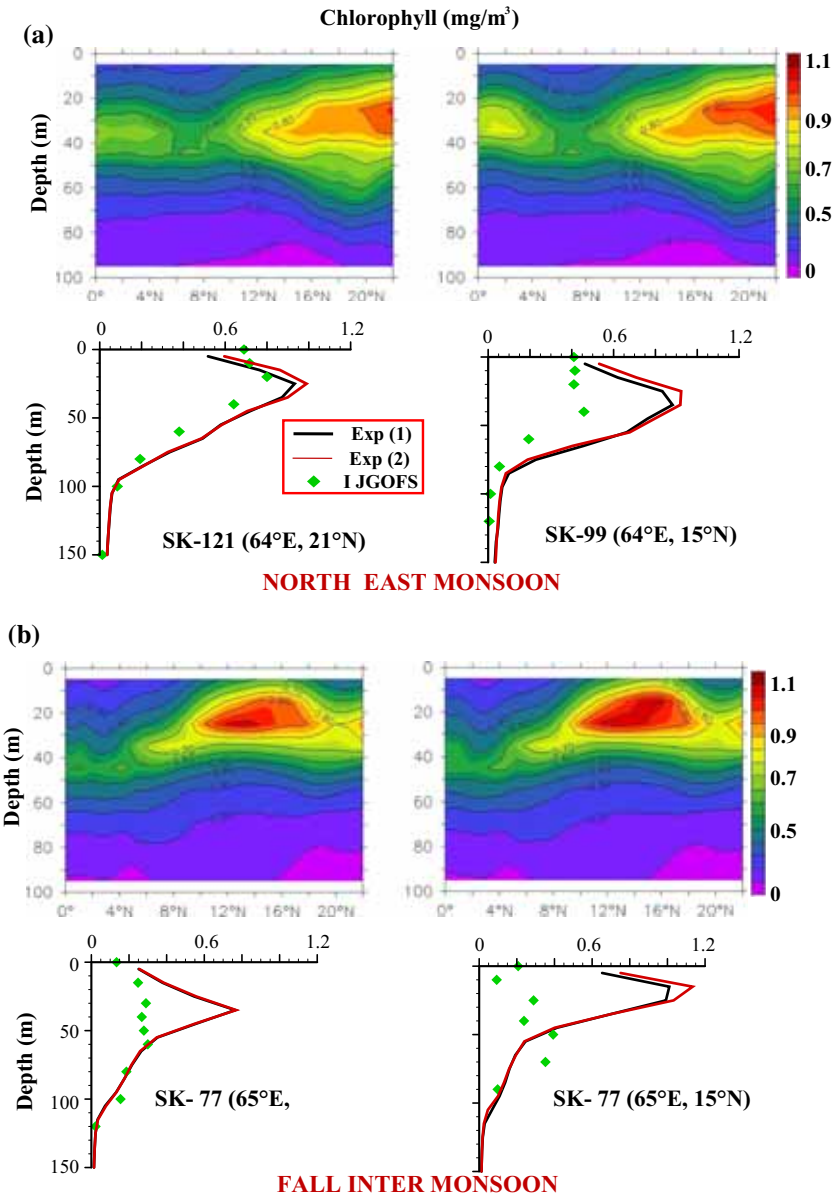

Figure 3. Latitudinal variation of chlorophyll (mg/m^3) with respect to depth along 65°E for Exp (1) and Exp (2) and comparison of profiles of chlorophyll at two stations in the Arabian Sea during NEM and FIM.

at the surface, etc., using data from satellites (TMI: apdrc.soest.hawaii.edu, Moderate Resolution Imaging Spectroradiometer (MODIS) and Sea-viewing Wide Field-of-view-Sensor (SeaWiFS): https://oceancolor.gsfc.nasa.gov), cruises (US JGOFS: http://usjgofs.whoi.edu and Bay of Bengal Process studies from NIO, Goa) and World Ocean Atlas (WOA: nodc.noaa.gov/OC5/WOA05/woa05data.html) in the Arabian Sea and the Bay of Bengal. It was noted that results of model simulations were able to capture significant features of spatial, seasonal and interannual variations of many of the biogeochemical components in the north Indian Ocean when compared with the available data. Also, model simulation results have been analysed in detail to understand the various physical, biological and chemical processes which influence the spatial and seasonal variations of PP in the north Indian Ocean. The reader is referred to the two studies cited earlier for more details.

3. Analysis and discussion of model simulation results

In this paper, the results of two numerical simulations of TOPAZ model (Exp (1) and (2)) with climatological and interannual forcings are analysed for different regions in the Arabian Sea (AS) and the Bay of Bengal (BOB). Four seasons: North East Monsoon, NEM – December, January, February; Spring Intermonsoon, SIM – March, April, May; South West Monsoon, SWM – June, July, August; Fall Intermonsoon, FIM – September, October, November are considered for analysis. Evaluation of model simulation results of Chl, PP, nutrients and pCO_2 is carried out using data from different sources (WOA, US JGOFS Arabian Sea Process Studies cruises, Indian JGOFS cruises, SeaWiFS and MODIS satellites) in the north Indian Ocean for spatial, seasonal and interannual variations.

Figure 1(a and b) shows the spatial variation of PP in the euphotic zone and nitrate (NO_3) in the upper 50 m from two numerical simulations (Exp (1) and (2)) with climatological forcing and PP from satellite data (SeaWiFS) and NO_3 from World Ocean Atlas in the AS and BOB during two seasons, namely, NEM and FIM (Results for SIM and SWM are not shown). The PP is estimated using the VGPM of Behrenfeld and Falkowski (1997) from SeaWiFS data of chlorophyll, available light and photosynthetic efficiency. It is noticed that higher PP is obtained for Exp (2) compared to Exp (1) in west and north-west AS (since iron limitation for Exp (2) is less than Exp (1)) and Exp (2) compares well with satellite data. Also, NO_3 at the surface is less for Exp (2) compared to Exp (1) when PP is high for Exp (2) (since utilization of NO_3 for PP is high).

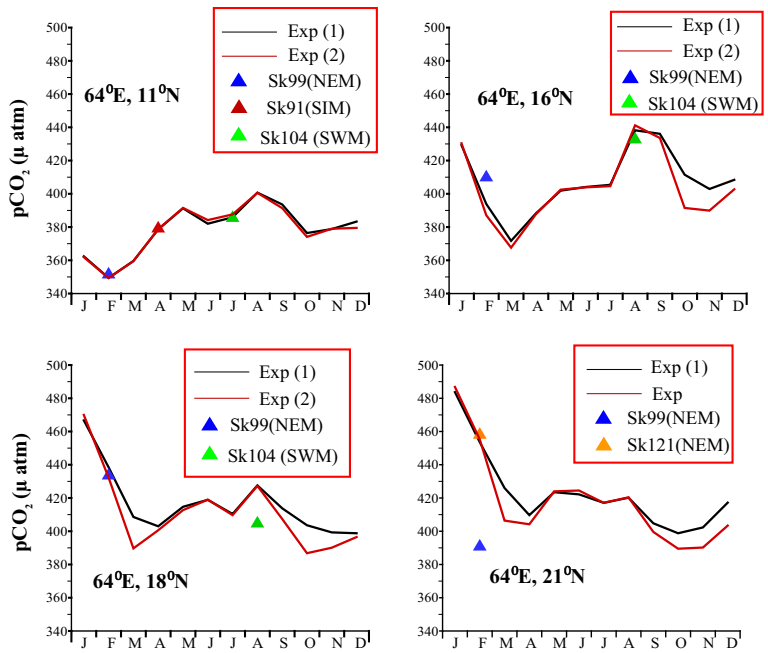

Figure 4. Comparison of pCO2 (μatm) from model simulations Exp (1) and (2) with Indian JGOFS cruise data at four stations in the Arabian Sea.

The pCO_2 is estimated from the model simulation results using dissolved inorganic carbon (DIC), alkalinity (Alk) at a particular temperature (T) and salinity (S) using an initial guess for the total hydrogen as per OCMIP-2 protocol (Najjar and Orr 1998) to solve the reaction equations of the carbonate system iteratively. Spatial variation of pCO_2 at the surface for two seasons, NEM and FIM (figure 1c) shows that model results capture the trend observed in the available data from Takahashi *et al.* (2002) and pCO_2 is less for Exp (2) in the west AS and southern coast of India where PP is high and more carbon is fixed.

It is also observed that variations in PP due to change in Fe limitation parameter are not the same in different regions of AS and BOB. Therefore, detailed analysis of temperature, salinity, PP, Chl and nutrients is carried out in different regions in AS and BOB. Figure 2 shows the regions of study in AS and BOB and table 1 indicates the extent of regions.

Model results have been now validated for many of the biogeochemical components and fluxes, using data from Indian JGOFS and US JGOFS cruises at several stations in the AS. Figure 3 shows the latitudinal variation of Chl with respect to depth along 65°E and comparison of profiles of Chl at two stations in the AS during NEM and FIM (figures not shown for SIM and SWM) with Indian JGOFS data. It is noticed from the model results that subsurface chlorophyll maximum (SCM) exists at all latitudes along 65°E transect during all the four seasons and its magnitude increases towards north from 6° to 22°N during NEM and is maximum between 12° and 16°N during FIM. Chl values obtained from model simulations are in agreement with the Indian JGOFS data during NEM and SWM (not shown) and are higher than Indian JGOFS data during SIM (not shown) and FIM.

In figure 4, monthly variation of pCO_2 from model simulation results for Exp (1) and (2) are compared with available data from Indian JGOFS cruises at several locations along 65°E transect. As expected, from figures 1(c) and 4, it is observed that pCO_2 for Exp (2) is less than Exp (1) during February and March and September to December at all stations north of 14°N (when there is Fe limitation), since PP is higher and fixation of carbon is more for Exp (2) in the north AS. Also model results for Exp (2) compare well with the cruise data.

It is seen in figure 5(a) that profiles of seasonal average values of Fe from the model for two seasons, namely, SWM and FIM at four stations in AS capture the depthwise variations observed in data from US JGOFS cruises in the upper 100 m. In figure 5(b), seasonal average values of silicate (Si) from the model simulations are compared with data from Indian JGOFS Cruises at four stations and during three seasons. It is noticed that model simulation results match well with the data. Also, concentrations of Fe and Si are same for both Exp (1) and (2) along 65°E, since difference in multi-nutrient limitation determined by Liebig Limitation (refer equations 26–37 in Dunne *et al.* 2010) for the two numerical experiments is not of considerable magnitude in east and central Arabian Sea. Discrepancies in the model results when

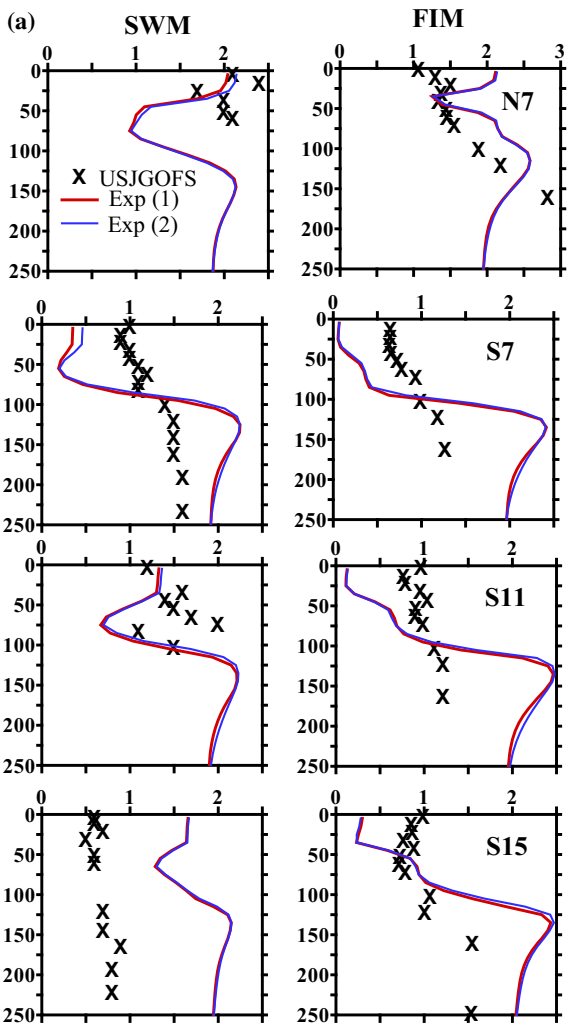

Figure 5. (**a**) Profiles of iron (nMol/m^3) from two model simulations compared with US JGOFS cruise data during two seasons, SWM and FIM at 4 stations in the Arabian Sea: Stations – N7: 67°E, 19°N, S7: 62°E, 16°N, S11: 65°E, 14.5°N, S15: 65°E, 10°N. (**b**) Profiles of silicate (mMol/m^3) from two model simulations compared with Indian JGOFS cruise data during three seasons, NEM, SIM and SWM at four stations in the Arabian Sea.

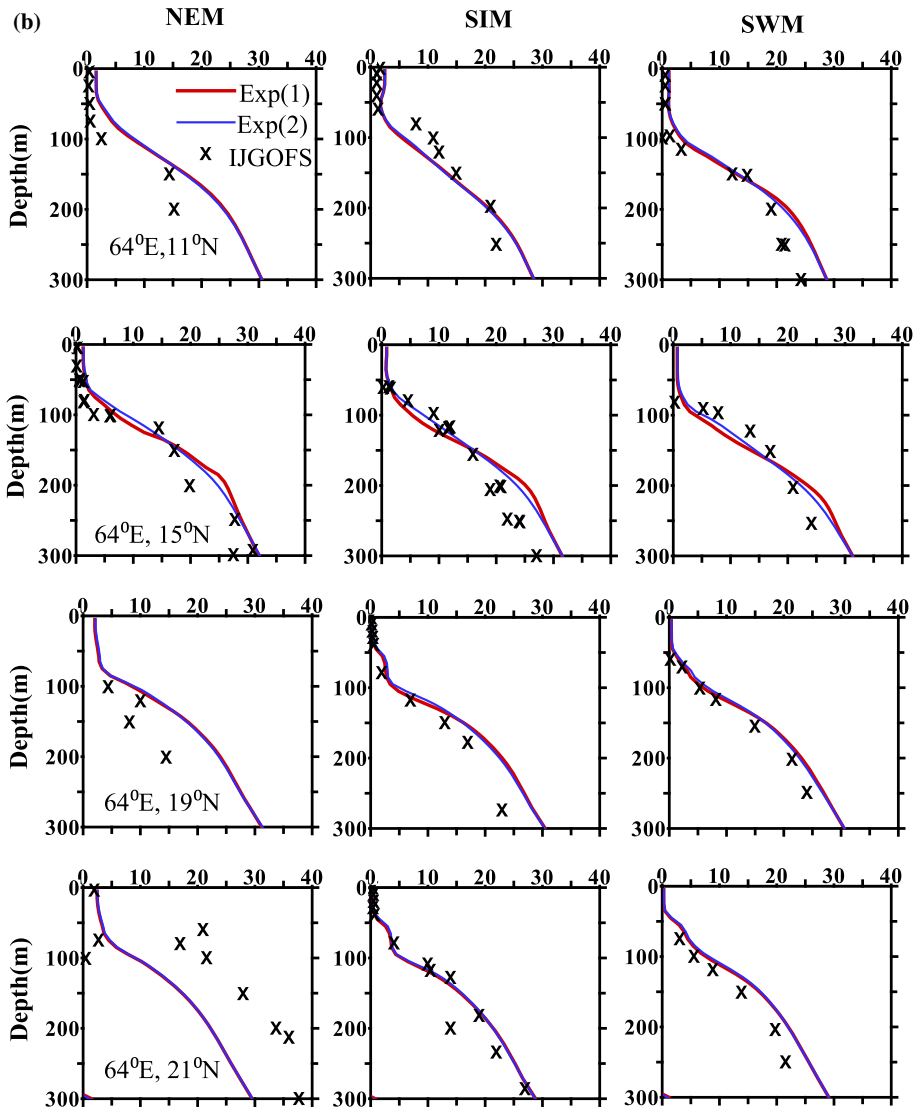

Figure 5. (*Continued.*)

compared with observations may be attributed to the model resolution and parameters related to various process models.

Depthwise variations of Chl and PP for all regions of AS for Exp (1) and (2) (climatological simulations) show that Chl and PP are more for Exp (2) during all seasons in the north and west AS. In these regions, it is noticed that nutrients like NO_3, Ammonium (NH_4) and Fe in the upper 50 m are less for Exp (2) compared to Exp (1) since PP and nutrient utilization are higher for Exp (2). In the east AS (east of 65°E), depthwise variations of Chl and PP for Exp (1) and (2) look similar indicating that Fe limitation parameter does not affect Chl or PP (figures not shown).

Marine biogeochemical model simulations are carried out for interannual variability by using CORE fluxes during the years 1949–2009. Detailed analysis of results of numerical simulations on various biogeochemical variables and fluxes are done for the period 1997–2009 in different regions of AS. Figure 6 shows the interannual variation of PP in the euphotic zone from two model simulations, Exp (1) and (2) compared with PP estimated from satellite data (MODIS and SeaWiFS, http://web.science.oregonstate.edu/ocean.productivity/) using Eppley VGPM in west AS (Region 1: refer table 1, figure 2). It is observed that seasonal and interannual variations of PP are significant, PP for Exp (2) is higher compared to Exp (1) (especially during September to November since Fe influences the uptake rates for large and small phytoplankton), and Exp (2) compares well with PP estimated from satellite data.

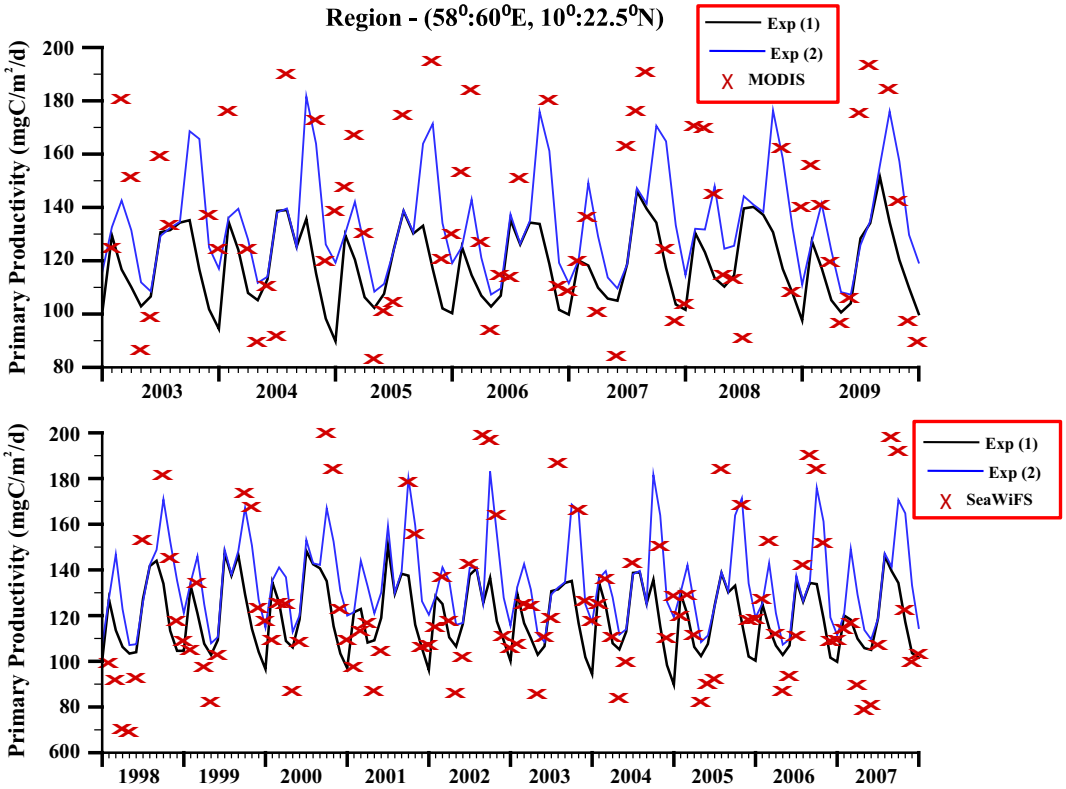

Figure 6. Interannual variation of primary productivity (mgC/m^2/d) in the euphotic zone from two model simulations, Exp (1) and (2) compared with PP estimated from satellite data (MODIS and SeaWiFS) using Eppley VGPM in the west Arabian Sea.

Further, detailed analysis of the two numerical simulation results on PP, Chl and nutrients are carried out for different regions in AS during El Nino and La Nina Years. Depthwise variation of PP, Chl, NO_3, NH_4, Fe and Si (not shown), during 2006–2008 for a region in west AS (Region 4D: 60°:65°E, 18°:20°N) are shown in figure 7(a and b). It is noticed that PP and Chl are higher (figure 7a) and NO_3 and NH_4 are lower for Exp (2) in the upper 100 m when compared to Exp (1) (figure 7b) because of higher nutrient utilization. Also, PP and Chl are higher during 2008 compared to 2007 since 2008 is influenced by La Nina event. Depthwise variation of PP and Chl during 2006–2008 shows that PP and Chl are higher during 2006 and 2008 compared to 2007 in all the regions in west and north-west AS. Satellite data on Chl and PP obtained from MODIS also shows higher surface Chl and PP during 2008.

Carbon flux is calculated in the model following the OCMIP-2 protocol using difference of pCO_2 between ocean and atmosphere, and gas transfer velocity (Najjar and Orr 1998; Sharada *et al.* 2008; Kanuri *et al.* 2017). Figure 8 shows monthly variation of pCO_2 and carbon flux (atmospheric pCO_2 used for calculation of carbon flux is 360 µatm) from ocean to atmosphere during 2006–2008 for the same region (Region 4D) and it is seen that pCO_2 and carbon flux from ocean to atmosphere (figure 8) for Exp (2) is lower since PP is high. However, study on correlations between ocean surface pCO_2 and surface chlorophyll by Fay and McKinley (2013) reveals the time scales on which primary productivity can directly modify the oceanic carbon uptake in five biomes in the World Ocean, but this study does not include the domain of our present study.

Table 2 provides an overview of the annual average of PP for two model simulations Exp (1) and (2) in different regions of AS and BOB, and comparison of PP (Eppley VGPM) estimated using SeaWiFS and MODIS satellite data (Note: Annual average of PP from model simulation results for (i) 1998–2007 is considered for comparison with SeaWiFS data and (ii) 2003–2009 is considered for comparison with MODIS data). It is noted that PP is higher for Exp (2) compared to Exp (1) in the regions west of 65°E in the AS and PP is almost same for Exp (1) and (2) in the regions east of 65°E and whole of BOB. Also, PP

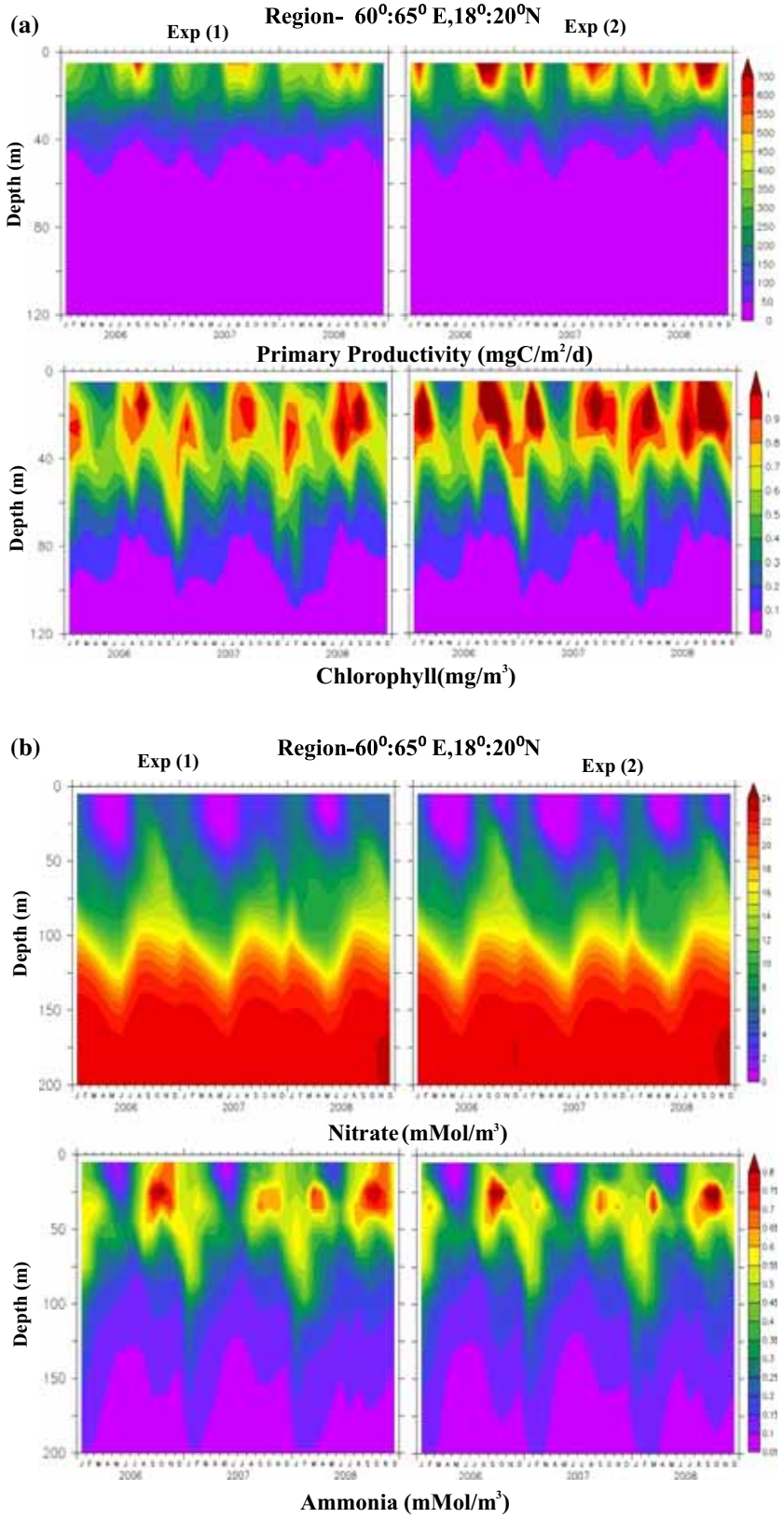

Figure 7. Depthwise variation of (**a**) primary productivity (mgC/m^2/d) and chlorophyll (mg/m^3) and (**b**) nitrate (mMol/m^3) and ammonia (mMol/m^3) during 2006–2008 for Region 4D in the Arabian Sea for two model simulations.

from Exp (2) compares well with satellite data in many regions of AS, whereas it is overestimated in BOB. Gomes *et al.* (2016) state that phytoplankton biomass obtained from satellites in the Bay of Bengal are of limited use because of cloud cover, heavy fresh water discharges from

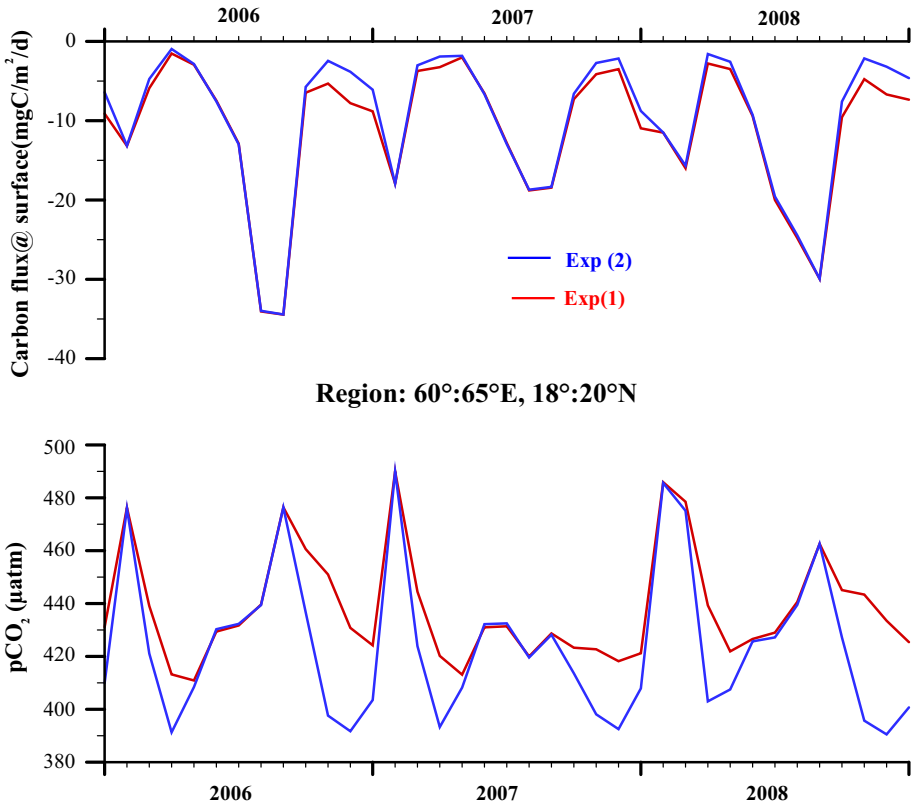

Figure 8. Comparison of interannual variation of pCO_2 (µatm) and carbon flux (mgC/m^2/d) from model simulations Exp (1) and Exp (2) during 2006–2008 for Region 4D.

rivers, and considerable fraction of phytoplankton in the euphotic zone is at depth which are not captured by satellite measurements. Also, other modelling studies have noticed discrepancies while comparing model outputs on chlorophyll with satellite data in Bay of Bengal. It can also be seen from the table that PP estimated from MODIS is more than PP estimated from SeaWiFS in the north-west regions of the AS.

To understand the effect of iron limitation parameter on PP, detailed analysis of the deficiency of iron (i.e., chlorosis factor which is a function of Fe:N ratio, which modulates Chl:N ratio; Dunne *et al.* 2010), Liebig limitation for nutrient uptake, specific growth rates for large and small phytoplankton are carried out. It is noted that if $(Fe:N)_{irr}$ is decreased, chlorosis is increased (i.e., iron limitation is reduced), specific growth rate for large and small phytoplankton are increased (please refer to the equations provided in the appendix, equations 26–37 in Dunne *et al.* 2010)). Figure 9 shows the Total PP, PP of large phytoplankton, PP of small phytoplankton, and the terms which are responsible for determining the specific growth rate of phytoplankton for Exp (1) and Exp (2) during February and November for one region 3A in the west AS (figure 9a) and one region 2C in the east AS (figure 9b). It is clearly seen that when PP is higher for Exp (2) compared to Exp (1) (during some months) in the west AS, specific growth rate, Liebig limitation and chlorosis (Def_fe) are higher for both large and small

Table 2. *Annual average of primary productivity (mgC/m^2/d).*

	Exp (1)		Exp (2)		SeaWiFS	MODIS
Region	98-07	03-09	98-07	03-09	98-07	03-09
1	1194	1187	1348	1342	1434	1539
2A	1075	1070	1116	1113	908	839
2B	979	956	979	956	737	671
2C	1009	989	1010	989	886	789
2D	1102	1087	1163	1165	1048	1054
3A	1085	1075	1227	1232	1181	1201
3B	1076	1065	1079	1066	1009	900
4A	1105	1098	1115	1104	1073	973
4B	1216	1209	1332	1312	1516	1649
4C	1334	1321	1429	1413	1948	2240
4D	1117	1114	1304	1290	1311	1459
5	1381	1368	1428	1416	1939	2469
6	1076	1079	1107	1113	851	815
7	993	991	1038	1031	898	856
8	1039	1041	1070	1070	980	960

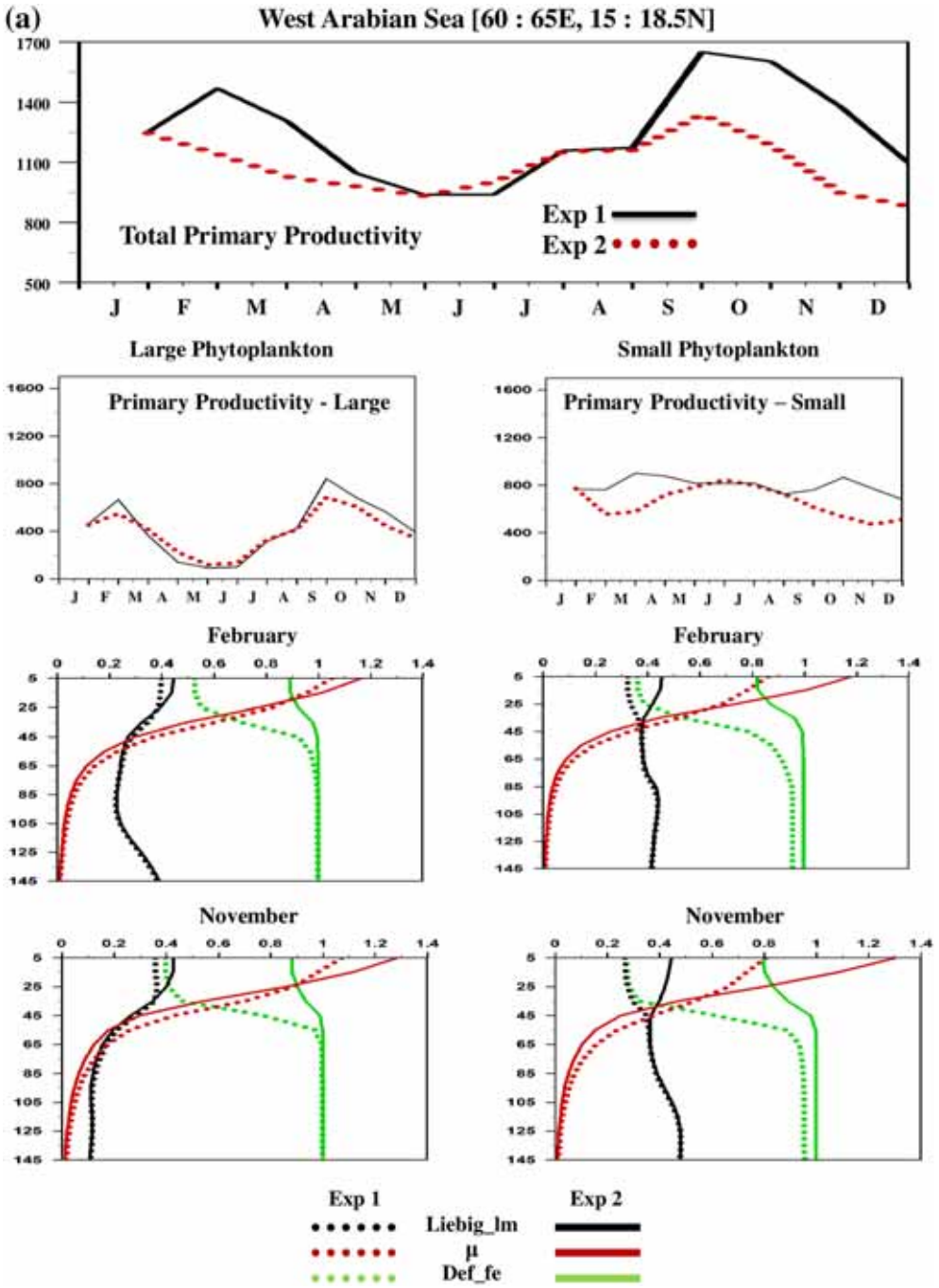

Figure 9. Comparison of primary productivity and terms related to specific growth rate of large and small phytoplankton (Liebig limitation and Def_fe or chlorosis) from model simulations Exp (1) and Exp (2) in the (**a**) west Arabian Sea (Region 3A) and (**b**) east Arabian Sea (Region 2C).

phytoplankton (figure 9a) and also, the effect of iron limitation parameter is higher for small phytoplankton compared to large phytoplankton. Further, there is no change observed in PP when $(Fe:N)_{irr}$ is decreased in the regions east of 65°E in the AS (figure 9b) since there is no change in Liebig limitation and hence, specific growth rates of small and large phytoplankton.

4. Conclusions

The present study clearly indicates that the trace element iron plays a significant role in altering the nutrient cycles, primary production by phytoplankton, marine pCO_2 and therefore the air–sea carbon flux in the north and north-west regions of the Arabian Sea based on the analysis of model

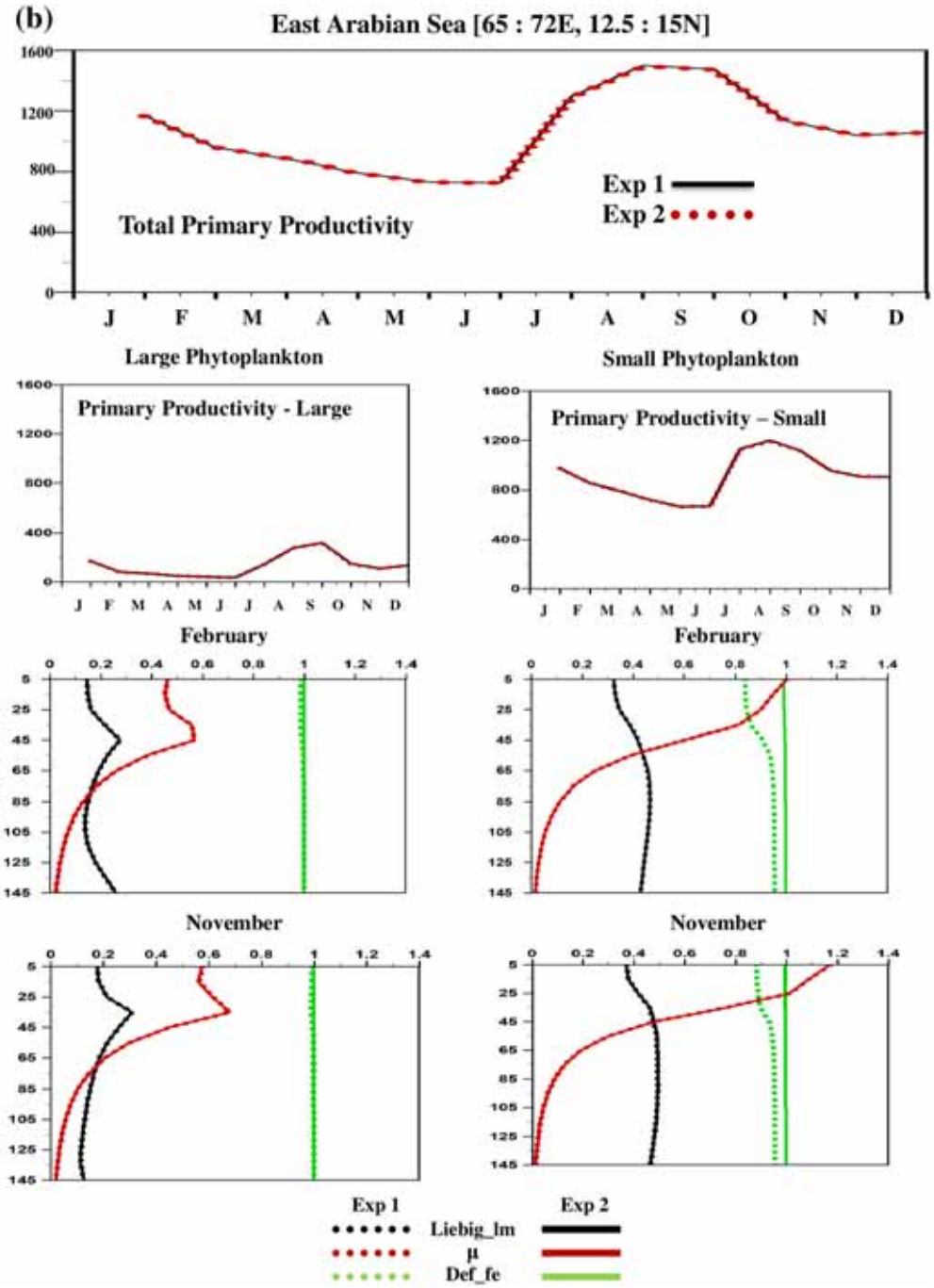

Figure 9. (*Continued.*)

simulation results of biogeochemical variables and fluxes for monthly, seasonal and interannual variations. It is noticed that PP and Chl increase, NO_3 and pCO_2 decrease during January–March and September–December, when iron limitation is reduced (i.e., light utilization efficiency is altered) in the north and north-west regions of the Arabian Sea. But in the east Arabian Sea and regions of Arabian Sea south of 10°N, PP, Chl, NO_3 and pCO_2 did not show any change when iron limitation parameter is varied. Analysis of the sensitivity of iron limitation parameter to processes required to determine PP clearly indicates that specific growth rates for large and small phytoplankton are altered when iron limitation parameter is varied. Also, model simulation results on PP, Chl, SST are able to capture the interannual variability due to ENSO events like El Nino and La Nina.

Acknowledgements

The authors gratefully acknowledge the data sources for this study: the World Ocean Database, the World Ocean Atlas 2005, CORE-data products, Ocean colour from the MODIS and SeaWiFs projects, NASA/Goddard Space Flight Center (www.oceandata.sci.gsfc.nasa.gov), and Oregon State University Ocean Primary productivity home page. The authors also wish to thank the developers of MOM4p1 (Griffies and the team from GFDL) and Ferret for graphic outputs. The authors thank cruise data of Indian JGOFS programme and Chris Measures for providing the access to US JGOFS cruise data on US JGOFS home page. Authors wish to thank Head, CSIR-4PI for encouragement and High Performance Computational Systems Group at CSIR-4PI for computational support. The model simulations are carried out on CSIR-4PI Supercomputer Ananta. The project is partially funded by Ministry of Earth Sciences (MOES) India and CSIR under ARiEES Project. Also, C Kalyani Devasena acknowledges DST-WOS fellowship. Funding was provided by (i) Council of Scientific and Industrial Research, (ii) Ministry of Earth Sciences, and (iii) Department of Science and Technology, India.

Appendix

Fe:N ratio modulates the Chl:N ratio through 'Chlorosis (χ)' factor and Fe:N ratio of phytoplankton is normalised to saturated value $(\mathrm{Fe{:}N})_{\mathrm{irr}}$ necessary to synthesise chlorophyll (Sunda and Huntsman 1997)

$$\chi = \frac{(\mathrm{Fe:N})^2}{\left[(\mathrm{Fe:N})^2_{\mathrm{irr}} + (\mathrm{Fe:N})^2\right]} = \frac{\mathrm{Fe}^2}{\left[(\mathrm{Fe:N})^2_{\mathrm{irr}} \cdot \mathrm{N}^2 + \mathrm{Fe}^2\right]} \tag{1}$$

Chlorosis affects the Chl:C ratio (Geider *et al.* 1997)

$$\mathrm{Chl:C} = \theta = \frac{\theta_{\max}}{\left[1 + \theta_{\max} \cdot \frac{\alpha I}{2 \cdot P_{C_m}}\right]} \cdot \chi \tag{2}$$

or, alternatively, Liebig-type formulation

$$\theta = \min\left(\frac{\theta_{\max}}{\left[1 + \theta_{\max} \cdot \frac{\alpha I}{2 \cdot P_{C_m}}\right]}, \theta_{\max} \cdot \chi\right) \tag{3}$$

Growth rates for small and large phytoplankton, diazotrophs are then calculated (Dunne *et al.* 2010) as

$$\mu = \frac{P_{C_m}}{(1+\zeta)} \cdot \left(1 - e^{\left(-\alpha \cdot I \cdot \mathrm{Chl:C}/P_{C_m}\right)}\right). \tag{4}$$

The complete set of equations are available in Dunne *et al.* (2010).

References

Behrenfeld M J and Falkowski P G 1997 Photosynthetic rates derived from satellite-based chlorophyll concentration; *Limnol. Oceanogr.* **42(1)** 1–20.

Behrenfeld M J, Westberry T K, Boss E S, O'Malley R T, Siegel D A and Wiggert J D *et al.* 2009 Satellite-detected fluorescence reveals global physiology of ocean phytoplankton; *Biogeosci.* **6** 779–794.

Boyd P W, Jickells T, Law C S, Blain S, Boyle E A and Buesseler K O *et al.* 2007 Mesoscale iron enrichment experiments 1993–2005: Synthesis and future directions; *Science* **315** 612–617, https://doi.org/10.1126/science.1131669.

Buesseler K O, Doney S C, Karl D M, Boyd P W, Caldeira K and Chai F *et al.* 2008 Ocean iron fertilization – moving forward in a sea of uncertainty; *Science* **319** 162, https://doi.org/10.1126/Science.1154305.

Cullen J J 1995 Status of the iron hypothesis after the Open-Ocean Enrichment Experiment; *Limnol. Oceanogr.* **40** 1336–1343.

Dunne J P, Gnanadesikan A, Sarmiento J L and Slater R D 2010 Technical description of the prototype version (v0) of tracers of phytoplankton with Allometric Zooplankton (TOPAZ) ocean biogeochemical model as used in the Princeton IFMIP model; *Biogeosci.* **7**(**Suppl-3593**) 1–22.

Dutkiewicz S, Follows M J and Parekh P 2005 Interactions of the iron and phosphorus cycles: A three-dimensional model study; *Global Biogeochem. Cycles* **19**, https://doi.org/10.1029/2004GB002342.

Fay A R and McKinley G A 2013 Global trends in surface ocean pCO_2 from *in-situ* data; *Global Biogeochem. Cycles* **27** 541–557, https://doi.org/10.1002/gbc.20051.

Gautam R, Liu Z, Singh R P and Hsu N C 2009 Two contrasting dust-dominant periods over India observed from MODIS and CALIPSO data; *Geophys. Res. Lett.* **36** L06813, https://doi.org/10.1029/2008gl036967.

Geider R J, MacIntyre H L and Kana T M 1997 Dynamic model of phytoplankton growth and acclimation: Responses of the balanced growth rate and the chlorophyll *a*: Carbon ratio to light, nutrient-limitation and temperature; *Mar. Ecol. Prog. Ser.* **148** 187–200.

Gnanadesikan A, Sarmiento J L and Slater R D 2003 Effects of patchy ocean fertilization on atmospheric carbon dioxide and biological production; *Global Biogeochem. Cycles* **17(2)**, https://doi.org/10.1029/2002GB001940.

Gomes H do, deRada R S, Goes J I and Chai F 2016 Examining features of enhanced phytoplankton biomass in

the Bay of Bengal using a coupled physical-biological model; *J. Geophys. Res. Oceans* **121** 5112–5133, https://doi.org/10.1002/2015jc011508.

Griffies Stephen M 2007 Elements of MOM4P1; Tech Rep. **6** Princeton, NJ, GFDL Ocean Group.

Griffies Stephen M, Arne Biatoch and Claus Boning *et al.* 2009 Coordinated Ocean-ice Reference Experiments (COREs); *Ocean Model.* **26** 1–46, https://doi.org/10.1016/j.ocemod.2008.08.007.

IPCC 2007 *Climate Change 2007: Impacts, adaptation and vulnerability contribution of Working Group II to the Fourth Assessment Report of the IPCC* (eds) Parry M L, Canziani O F, Palutikof J P, Van der Linden P and Hanson C E, Cambridge University Press, Cambridge, UK, 976p.

Kalyani Devasena C, Sharada M K, Swathi P S and Yajnik K S 2014 Evaluation of biogeochemical model simulations using World Ocean Atlas and satellite observations in the Arabian Sea; *Int. J. Remote Sensing* **35(14)** 5448–5458.

Kanuri V V, Gijjapu D R and Munnooru K *et al.* 2017 Scales and drivers of seasonal pCO_2 dynamics and net ecosystem exchange along the coastal waters of southeastern Arabian Sea; *Mar. Pollut. Bull.* **121** 372–380.

Kayetha V K, Kumar J S, Prasad A K, Guido Cervone and Singh R P 2007 Effect of dust storm on ocean color and snow parameters; *J. Indian Soc. Remote Sens.* **35** 1–9, https://doi.org/10.1007/BF02991828.

Large W, McWilliams J and Doney S 1994 Oceanic vertical mixing: A review and a model with nonlocal boundary layer parameterization; *Rev. Geophys.* **32** 363–403.

Martin J H and Fitzwater S E 1988 Iron deficiency limits phytoplankton growth in the north east Pacific subarctic; *Nature* **331** 341–343.

Martin J H, Gordon R M, Fitzwater S E and Broenkow W W 1989 VERTEX: Phytoplankton/iron studies in the Gulf of Alaska; *Deep Sea Res.* **36** 649–680.

Measures C I and Vink S 1999 Seasonal variations in the distribution of Fe and Al in the surface waters of the Arabian Sea; *Deep-Sea Res. Part-II* **46** 1597–1622, https://doi.org/10.1016/S0967-0645(99)00037-5.

Moore J K, Doney S C and Indsay K L 2004 Upper ocean ecosystem dynamics and iron cycling in a global three-dimensional model; *Global Biogeochem. Cycles* **18** GB4028, https://doi.org/10.1029/2004GB002220.

Moffett J W, Vedamati J, Goepfert T J, Pratihary A K, Gauns M and Naqvi S W A 2015 Biogeochemistry of iron in the Arabian Sea; *Limnol. Oceanogr.* **60** 1671–1688, https://doi.org/10.1002/lno.10132.

Naqvi S W A, Moffett J W, Gauns M U, Narvekar P V, Pratihary A K, Naik H and Shenoy D M *et al.* 2010 The Arabian Sea as a high nutrient, low-chlorophyll region during the late southwest monsoon; *Biogeosciences* **7** 2091–2100.

Najjar R and Orr J C 1998 Design of OCMIP-2 simulations of chlorofluorocarbons, the solubility pump and common biogeochemistry; Internal OCMIP Report, *Lab. Des Sci. du Clim. et de l'Environ., Comm. A l'Energie, Atom.,* Gif-sur-Yvette, France, 25p.

Resplandy L, Levy M, Madec G, Pous S, Aumont O and Kumar D 2011 Contribution of mesoscale processes to nutrient budgets in the Arabian Sea; *J. Geophys. Res. Oceans* **116** C11007, https://doi.org/10.1029/2011JC007006.

Sarmiento J L, Murnane R J and Quere C L 1995 Air–sea CO_2 transfer and the carbon budget of the North Atlantic; *Phil. Trans. Roy. Soc.-B Biol. Sci.* **348(1324)** 211–219, https://doi.org/10.1098/rstb.1995.0063.

Sharada M K, Yajnik K S and Swathi P S 2005 Evaluation of six relations of the kinetics of uptake by phytoplankton in multi-nutrient environment using JGOFS experimental results; *Deep Sea Res. II* **14–15** 1892–1909.

Sharada M K, Swathi P S, Yajnik K S and Kalyani Devasena C 2008 Role of biology in the air–sea carbon flux in the Bay of Bengal and Arabian Sea; *J. Earth Syst. Sci.* **117** 429–447.

Sharada M K, Kalyani Devasena C, Swathi P S, Sundara Deepthi M V, Shelva Srinivasan M K and Yajnik K S 2015 Seasonal and interannual vaiariability of marine ecosystem in the north Indian Ocean: A model Evaluation study; *Int. J. Ocean Climate Syst.* **6** 19–34.

Singh R P, Prasad A K, Kayetha V K and Kafatos M 2008 Enhancement of ocean parameters associated with dust storms using satellite data; *J Geophys. Res.* **113**, C11008, https://doi.org/10.1029/2008JC004815.

Smetacek V and Naqvi S W A 2008 The next generation of iron fertilization experiments in the Southern Ocean; *Phil. Trans. Roy. Soc. A* **366(1882)** 3947–3967, https://doi.org/10.1098/rsta.2008.0144.

Sunda W G and Huntsman S A 1997 Interrelated influence of iron, light and cell size on marine phytoplankton growth; *Nature* **390** 389–392.

Takahashi T, Sutherland S C, Sweeney C, Poisson A and Metzl N *et al.* 2002 Global sea–air CO_2 flux based on climatological surface ocean pCO_2, and seasonal biological and temperature effects; *Deep Sea Res., Part-II* **49(9–10)** 1601–1622.

Wiggert J D and Murtugudde R G 2007 The sensitivity of the southwest monsoon phytoplankton bloom to variations in aeolian iron deposition over the Arabian Sea; *J. Geophys. Res. Oceans* **112(C5)** C05005, https://doi.org/10.1029/2006jc003514.

Corresponding editor: C Gnanaseelan